Advances in magnetometry through miniaturization

A. S. Edelstein,[a] J. Burnette, and G. A. Fischer
U.S. Army Research Laboratory, 2800 Powder Mill Rd., Adelphi, Maryland 20783-1197

S. F. Cheng
U.S. Naval Research Laboratory, 4555 Overlook Ave., SW, Washington, DC 20375

W. F. Egelhoff, Jr., P. W. T. Pong, and R. D. McMichael
NIST, 100 Bureau Drive, Stop 1070, Gaithersburg, Maryland 20899-1070

E. R. Nowak
University of Delaware, Newark, Delaware 19716

(Received 5 May 2007; accepted 7 January 2008; published 30 June 2008)

Recent innovations may lead to magnetic sensors that are smaller, more sensitive, and/or cost less than current magnetometers. Examples of this are the chip scale atomic magnetometer, magnetic tunnel junctions with MgO barriers, and a device for minimizing the effect of $1/f$ noise, the microelectromechanical system (MEMS) flux concentrator. In the chip scale atomic magnetometer, researchers have been able to fabricate the light source, optics, heater, optical cell, and photodiode detector in a stack that passes through a silicon wafer. Theoretical and subsequent experimental work has led to the observation of magnetoresistance values of 400% at room temperature in magnetic tunnel junctions with MgO barriers. This large magnetoresistance occurs because electrons in the majority band can tunnel more easily through the MgO barrier than electrons in the minority band. The MEMS flux concentrator has the potential to increase the sensitivity of magnetic sensors at low frequencies by more than an order of magnitude. The MEMS flux concentrator does this by shifting the operating frequency to higher frequencies where the $1/f$ noise is much smaller. The shift occurs because the motion of flux concentrators on MEMS flaps modulates the field at kilohertz frequencies at the position of the sensor. Though miniaturization is generally beneficial, trade-offs are necessary because some properties, such as noise, worsen with decreasing size. © *2008 American Vacuum Society.* [DOI: 10.1116/1.2841516]

I. INTRODUCTION

Magnetic sensors have many applications[1] ranging from simply counting the rotations of parts in a car or assembly plant to such medical applications as magnetocardiography[2] and measuring brain activity. Compassing has been, and remains, an important use of magnetic sensors. A more recent application of magnetic sensors is in drug delivery. The type of magnetic sensor used depends on the application. For instance, the low cost Hall sensors used in the automotive industry to monitor various functions in cars are very different from the sensors used in hospitals to perform magnetic resonance imaging. The choice of magnetic sensor depends on cost, size, power consumption, frequency range, and sensitivity.

Magnetometers can be divided into two classes: vector magnetometers which measure the magnetic field in specific direction and total field or scalar magnetometers which measure the magnitude of the magnetic field. Scalar magnetometers[3] use the energy splittings between electronic or nuclear energy levels. The simplest and least sensitive total field magnetometer measures the nuclear precession rate in a magnetic field. A more sensitive total field magnetometer is the Overhauser effect magnetometer. In the Overhauser effect,[4] the polarization of electrons and the hyperfine interaction give rise to an enhanced nuclear polarization. At present, the most sensitive total field magnetometers are optically pumped magnetometers. A large magnetoresistance has been observed[5] at room temperature in semiconducting polymer sandwiches. What makes this work particularly interesting is that Francis *et al.* report that the magnetoresistance is independent of the direction of the magnetic field. A device using this effect could be a low cost total field sensor. At present, there are no low cost total field magnetic sensors.

The types of vector magnetometers include Hall effect, fluxgate, magnetoresistance, microelectomechanical system (MEMS), and coil based magnetometers. Each of these types can be further subdivided. For example, magnetoresistance sensors include anisotropic, giant magnetoresistance, and magnetic tunnel junction magnetoresistance sensors. Considerable progress has been made in making devices with increased magnetoresistance. Prior to the discovery[6,7] of giant magnetoresistance, the values of magnetoresistance (MR) were limited to those obtain by anisotropic MR (AMR) and were less than 3.5%. Room temperature MR values as large as 12.8% were observed[8] in giant MR (GMR) samples. Much larger values have been observed in magnetic tunnel junctions (MTJs). Initially, not much attention was paid to the matrix elements in tunnel junctions. For example, Julliere ignored their effect when he predicted[9] that the tunneling magnetoresistance ratio $\Delta R/R$ would be given by

[a]Electronic mail: edelstein@arl.army.mil

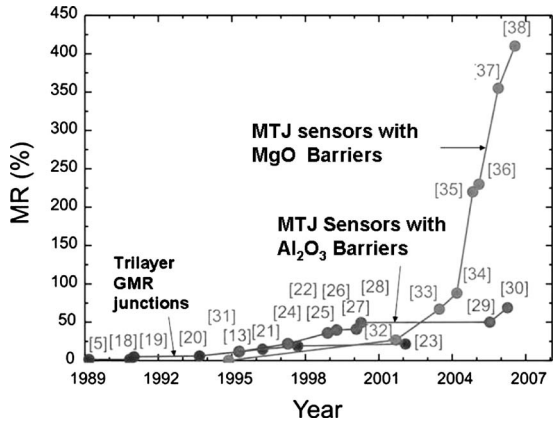

FIG. 1. Increase in MR vs time for GMR and MTJ junctions. Figure taken from Ref. 14. The numbers refer to references given in Ref. 14.

$$\Delta R/R = (R_a - R_p)/R_p = 2P_1P_2/(1 - P_1P_2), \quad (1)$$

where R_a and R_p are the resistances of the junction when the two ferromagnetic layers are antiparallel and parallel, respectively, and P_1 and P_2 are the spin polarizations of the two ferromagnets at the Fermi level. Butler *et al.*[10] and Mathon and Umerski[11] found that the tunneling conductance is strongly dependent on the symmetry of the electron states of the electrodes and the evanescent electron states in the barrier. This theoretical work motivated two groups[12,13] to study MTJs with MgO barriers. The increase in room temperature MR discussed by Heilger *et al.*[14] is illustrated in Fig. 1.

Figure 2 shows schematically some of the choices available in choosing magnetic sensors in terms of sensitivity and frequency. Table I compares some of the characteristics of these sensors. Total field sensors lose sensitivity with increasing frequency, whereas coil based sensors lose sensitivity at low frequency. At present, the most sensitive total field sensors are optically pumped sensors and the most sensitive commonly used vector sensors are fluxgates. One might think that vector sensors are always preferred since they provide more information. Actually, total field sensors are better on vehicles because they are insensitive to rotational vibrations. To see this, consider a rotation $d\theta$ of 0.1° of the axis of a vector sensor in the Earth's field B_E and that the angle between the axis of the sensor and the direction of the Earth's field is θ. This gives rise to a change $dB = -B_E \sin\theta d\theta$. For $\theta = 45°$ and $B_E = 50\,000$ nT, $dB = -62$ nT.

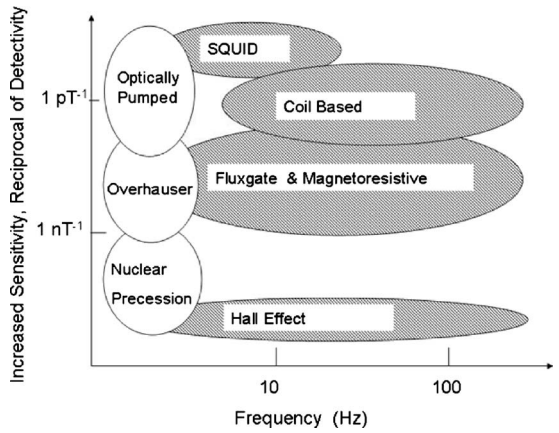

FIG. 2. Schematic of the detectivity vs frequency for several kinds of sensors. Sensors shown with a clear background are total field or scalar magnetometers. Sensors shown with a shaded background are vector magnetometers.

TABLE I. Comparison of the advantages and disadvantages of different types of magnetic sensors.

Type of Sensor	Advantages	Disadvantages
Total field sensors	Sensitive, insensitive to rotational Vibrations	Costly, best at low frequencies
Fluxgate	Sensitive	Costly, large, consumes a lot of power
Coil based	Sensitive at high frequencies	insensitive at low frequencies, costly, large
Magnetoresisitve	Low cost, small, potentially sensitive	$1/f$ noise

II. EXAMPLES OF PROGRESS IN MAGNETOMETRY

In this section, several examples of new developments of magnetometry will be discussed. One of the examples, the chip scale atomic magnetometer, is a scalar or total field magnetometer. The other examples are vector field magnetometers and the MEMS flux concentrator.

A. Chip scale atomic magnetometer

The chip scale atomic magnetometer is a miniaturization of optically pumped magnetometers. Optically pumped magnetometers typically have a cell containing Cs or Rb vapor.[3,15] Lasers are used to excite Cs or Rb atoms which then decay to the ground state, which is split into sublevels. All the atoms will end up in a sublevel which does not absorb light. With no other radiation present, the cell becomes transparent to the laser radiation. The energy splitting between the sublevels of the ground state is proportional to the magnitude of the magnetic field. If another radiation source is applied now whose photon energy matches the splitting, transitions between the sublevels in the ground state will occur and the cell will again absorb the laser radiation. Researchers[16] at NIST have been able to stack all the necessary components around a piece of silicon wafer, as illustrated in Fig. 3. Glass covers the top and bottom of the cell. Tin oxide heaters deposited on the glass covers are used to maintain the metallic vapor. The energy used in the heaters is the main energy requirement. Two laser sources are at the bottom of the stack. The radiation difference from these two sources provides the photons to allow the atoms in the excited state to relax to the ground state. The detectivity of the sensor is about 100 pT/$\sqrt{\text{Hz}}$ at 1 Hz. There are limits on decreasing the size of the cell because collisions with the cell

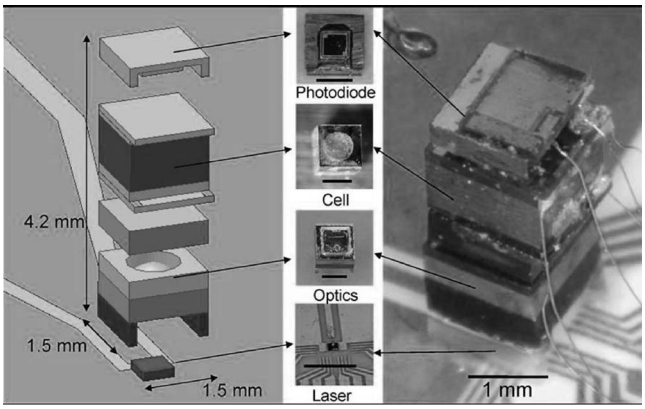

FIG. 3. Stack of elements in the chip scale atomic magnetometer. Kitching from NIST Boulder kindly supplied the figure.

walls limit the spin lifetime. A search is underway for materials to be used as cell liners that have a smaller effect on the spin lifetime.

B. Zigzag AMR sensor

The MR of AMR sensors depends on the angle ϕ between the current and the magnetization of a film of a ferromagnetic material such as Permalloy, an alloy of nickel and iron. AMR sensors have less $1/f$ noise than the other MR sensors. Because of this, they are widely used for low frequency applications. AMR sensors have a linear response when the angle ϕ is about 45°. Angled shorting strips in a "barber pole" configuration[17] are used to maintain ϕ approximately equal to 45°. Nevertheless, the direction of the magnetization tends to drift and this causes the sensitivity to change. Current pulses are sent through a coil to create field pulses that reset the direction of the magnetization. The need for these current pulses greatly increases the power required for AMR sensors. To prevent the drift, the ferromagnetic film can be deposited[18] in a zigzag pattern, as shown in Fig. 4. Because of shape anisotropy, the magnetization is in the plane of the film and tends to follow the zigzag pattern. The current tends to flow more in straight line path. Thus, shorting strips and currents for reset are avoided. One cannot reduce the scale of the device indefinitely because of the energy cost of creating domain walls. Silva *et al.*[18] quote a sensitivity of 3.54 mV/(V kA m^{-1}).

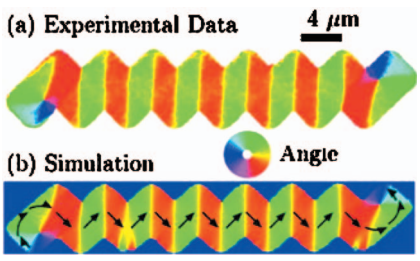

FIG. 4. (Color) Orientation of the magnetization in the zigzag AMR sensor. Figure taken from Ref. 18.

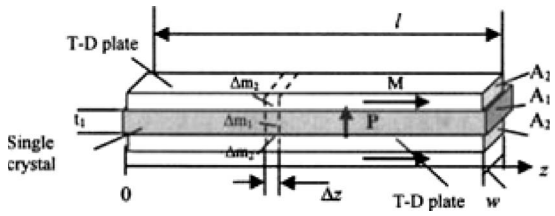

FIG. 5. Magnetoelectric sensor consisting of a piezoelectric material sandwiched between two layers of a magnetostrictive material. Figure supplied by Viehland.

C. Magnetoelectric sensor

Magnetoelectric sensors[19,20] are a clever arrangement of a piezeoelectric material sandwiched between two magnetostrictive slabs. In an applied field, the magnetostrictive material changes its length and strains the piezeoelectric material. Because of the strain, the piezeoelectric material generates a voltage. Thus, the sandwich generates a voltage without requiring power. Figure 5 illustrates the concept. Because the strains in magnetostrictive materials are even functions of the magnetic field, it is necessary to bias the sensor with a magnetic field. Using a MetGlas/polyvinylidene-fluoride laminate, Zhai *et al.* were able to detect[19] a 10 pT field at 48 kHz using an 8 Oe constant bias field.

D. MEMS flux concentrator

In this section, we describe the development of a device, the MEMS flux concentrator, designed to mitigate the effect of $1/f$ noise. As stated earlier, $1/f$ noise is a serious problem in magnetoresistance sensors.

1. Concept

The concept for the device has been presented previously.[21,22] Figure 6 shows a schematic of the device. Flux concentrators on MEMS flaps are on two sides of the magnetic sensor. The MEMS flaps are connected by springs so that there is a mechanical normal mode where the separation between the flaps oscillates. The MEMS flaps are driven to move at this normal mode by electrostatic comb drives. The motion of the MEMS flaps modulates the mag-

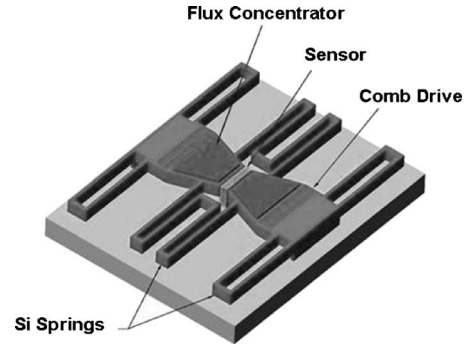

FIG. 6. Illustration of the concepts of the MEMS flux concentrator

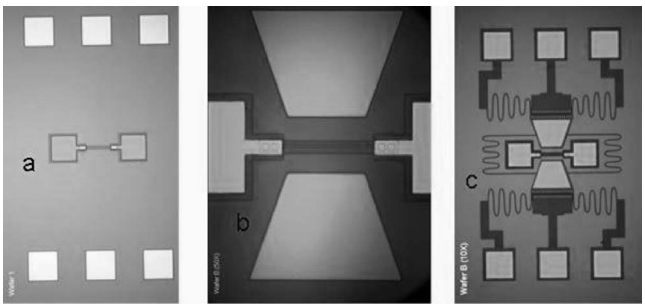

FIG. 7. Picture of the wafer after some of the processing steps. (a) After the gold electrodes and spin valve have been deposited. (b) After the flux concentrator has been deposited. (c) After the DRIE step but before release.

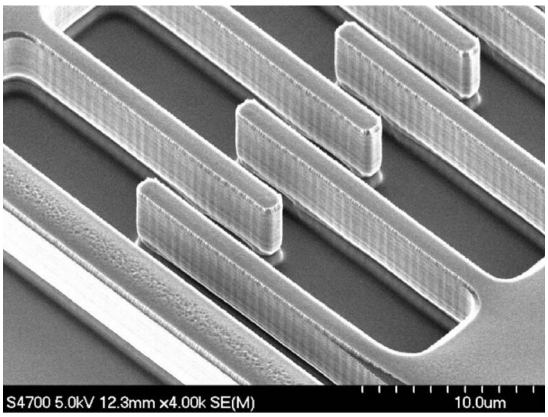

FIG. 8. Teeth of the electrostatic comb drive before release. The separation between the teeth is 2 μm.

netic field and, hence, shifts the operating frequency of the sensor to a higher frequency region where $1/f$ noise is much smaller.

2. Fabrication

The sensors used were spin valves, a type of four layer structure GMR sensor consisting of two ferromagnetic metallic layers separated by a conductor and an antiferromagnetic layer which is used to pin the magnetization of one of the ferromagnetic layers. The spin valves were supplied by NVE Corp. The flux concentrators were sputtered films consisting of two repeats of 40 Å Cr/1500 Å Permalloy.

The MEMS structures were prepared starting with silicon on insulator (SOI) wafers because using these wafers decreases the number of fabrication steps. However, the SOI wafers from several companies could not be used because the bonding through the SIO_2 layer between the device layer and the thick silicon part of the wafer, called the handle wafer, was not adequate. When we did the wet etch release in HF using these wafers, the etch rate was higher in the plane of the wafer and the anchors that support the MEMS structure were etched away. Fortunately, we were able to obtain some SOI wafers in which the bonding was good enough that the anchors survived the wet etch release. Best results were obtained when the device layer was 5 μm thick and the SiO_2 insulating layer was 3 μm thick. Gold electrodes were deposited and selected portions of the device layer were removed using deep reactive ion etching (DRIE). The MEMS structure was released using either a wet etch of HF followed by critical point drying or a dry HF vapor tool. To reduce the time required for the release, etch holes were made in the MEMS flaps. Figure 7 shows the wafer after some of the processing steps. In this early example of our process, there are no etch holes. Figure 8 shows the teeth of the comb drive before the MEMS structure is released. If a voltage is applied, the teeth are in a position of unstable electrostatic equilibrium. Because the separation between the teeth is only 2 μm, the springs of the MEMS structure must supply a strong symmetric restoring force. Figure 9 shows the MEMS structure moving at its resonant frequency of 15 kHz with a 12 μm amplitude. The amplitude of the drive voltage needed to get this amplitude was 50 V. By measuring the amplitude of the motion versus frequency, we determined that the Q of the resonant structure was about 30. We have gotten all the component parts to function correctly, but when we attempted to fabricate a complete device, we found that HF used in the wet HF release damaged the magnetic sensor. We were unable to find a suitable protective layer to prevent this damage. This led us to use flip chip bonding and to put the MEMS structure on one chip and the spin valve on the other chip. This approach allowed us to fabricate complete devices.

3. Testing

A picture of the complete package that has four devices, two of which are wired, is shown in Fig. 10. We analyzed the power spectrum of the output from the magnetic sensor in two ways. Sometimes, we measured it directly. Other times, we sent the output first to a lock-in amplifier whose switching frequency was controlled by the voltage source driving the MEMS structure. This second method allows us to demodulate the signal.

Each flap has a comb drive. If only one of the two comb drives is energized, then two major normal mode motions are possible. In one of the modes, the separation between the flaps stays constant and both flaps perform an oscillatory motion in the field sense direction of the magnetometer. We

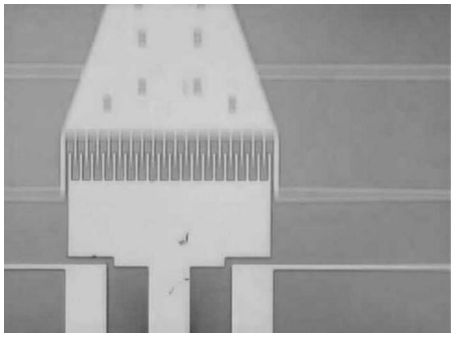

FIG. 9. Motion of the MEMS structure moving with an amplitude of 12 μm at the resonant frequency of 15 kHz.

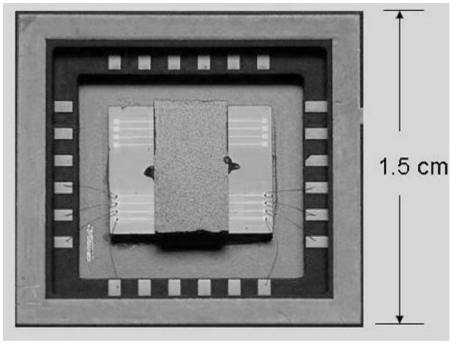

FIG. 10. Complete package containing four sensors completed using flip chip packaging.

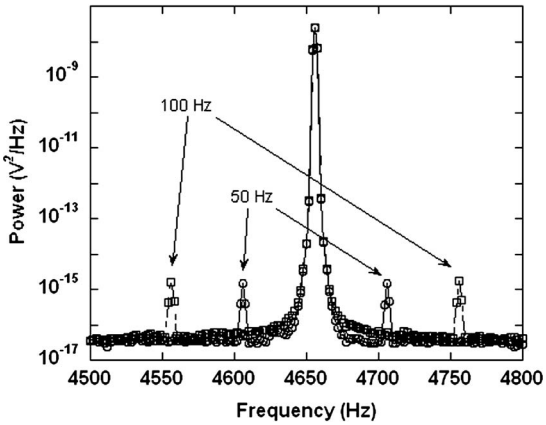

FIG. 11. Sidebands generated by applying a magnetic field at 50 and 100 Hz.

define this mode as the in phase mode. In the other mode, the flaps again perform an oscillatory motion in the field sense direction, but in this case, the separation between the flaps changes. We define this mode as the out of phase mode. If both comb drives are energized by the same voltage, only the out of phase mode occurs and the field at the position of the sensor is modulated. In our design, if the out of phase motion is driven to have an amplitude of 12 μm, we estimate that the magnetic field at the sensor will be modulated by a factor of 2. This estimate is based on magnetic field modeling calculations performed using MAXWELL 3D, a software package from Ansoft Corp. The reliability of these types of calculations was checked by comparing the results of model calculations and experiments using stationary flux concentrators.

We had already found[21] that the presence of the flux concentrator does not increase the noise. The reason that it does not increase the noise is because the flux concentrator is so much larger[23] than the spin valve. In testing the complete device, we found that applying the drive voltage does not increase the noise. When we applied magnetic fields at 50 and 100 Hz, sidebands to the applied drive signal were observed. These sidebands are shown in Fig. 11. Although this result was encouraging, it was noted that the amplitudes of these sidebands are too small. Apparently, the MEMS motion of the flaps is inhibited. We believe that the reason why the amplitude is too small is because the two chips are too close to one another. The separation will be increased in the next fabrication of the device. The amplitude of the sidebands in the power spectrum has the correct quadratic dependence on the magnitude of the field. Further, we found that we could demodulate a 1 Hz applied field even though the bandwidth of the signal applied to the MEMS flaps was 4 Hz wide. Thus, the bandwidth of the drive signal does not place a lower bound on the operating frequency of the device.

4. Plans and optimization

After obtaining the correct motion for the MEMS structure, the spin valve sensor will be replaced by MTJ sensors. One of the advantages of this sensor is that it has a bigger MR. The devices will be vacuum packaged to increase Q and, thus, decrease the necessary drive voltage. Vacuum packaging should increase the Q from 30 to about 300. The sensors should be used in a Wheatstone bridge configuration. To optimize the performance, one should consider all the noise sources. The noise sources include amplifier noise, Johnson and shot noises, electronic $1/f$ noise, magnetic white noise, and magnetic $1/f$ noise. Here, we shall only consider the magnetic noise. The $1/f$ noise, which is predicted[24] to be inversely proportional to the size of the system, will be decreased by the frequency shift provided for by the MEMS flux concentrator. Of more importance is the fact that the magnetic white noise[23] is also inversely proportional to the volume. Based on our estimates of possible performance, to obtain a detectivity of 1 pT/$\sqrt{\text{Hz}}$ at 1 Hz, it will be necessary to have a large volume for the free ferromagnetic layer in the MTJ sensor. The volume of the free layer can be made larger without changing the design of the MEMS flux concentrators by making the free layer thicker. MTJ sensors are better than GMR sensors for this application because one can increase the thickness of the free layer without affecting the sensitivity. One cannot increase the thickness of the free layer very much in GMR without decreasing their performance and/or making their impedance too low.

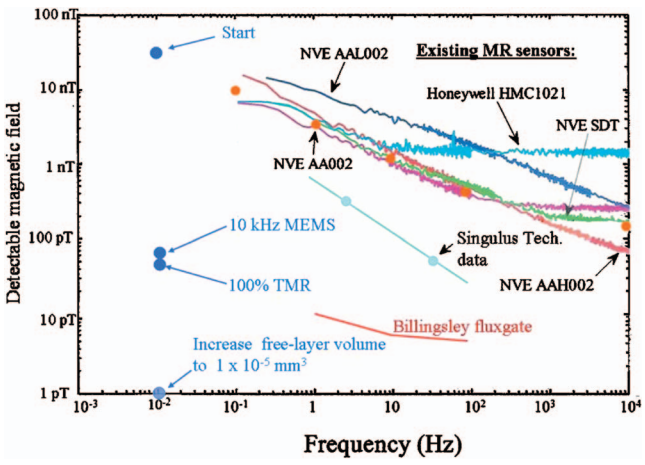

FIG. 12. (Color) Comparison of various vector magnetic sensors. The points at 10^{-2} Hz represent estimates of the field that we may be able to detect. Units for the y axis are magnetic field units/$\sqrt{\text{Hz}}$ at 1 Hz.

TABLE II. Definitions of the terms used in Eq. (2)

S_B	Sensor field noise power (T^2/Hz)
B_{sat}	Saturation field of free layer (T)
ΔR	Resistance change of one MTJ from parallel to antiparallel magnetization
R	Resistance of one MTJ in orthogonal magnetization state
N	Number of MTJs in each leg of the Wheatstone bridge.
V_J	Voltage drop across each MTJ.
V_i	V_J/N
S_v^{Amp}	Amplifier noise voltage power
S_v^{shot}	Shot-noise voltage power
$S_V^{\mathrm{elect}\ 1/f}$	Electronic $1/f$ noise voltage power
$S_B^{\mathrm{therm\ mag}}$	Thermal-magnetic noise field power
$S_M^{\mathrm{therm\ mag}}$	Thermal-magnetic noise magnetization power
$S_B^{\mathrm{mag}\ 1/f}$	Magnetic $1/f$ noise field power
e	Electronic charge
RAP	Resistance area product of each MTJ
A	Area of each MTJ
k_B	Boltzmann's constant
T	Absolute temperature
α_{elect}	Electronic $1/f$ Hooge parameter
f	Frequency of operation of MEMS flux concentrator
μ_o	Permeability of free space
α_G	Gilbert damping parameter
Ω	Free layer volume in each MTJ
γ	Gyromagnetic ratio for an electron
M_s	Saturation magnetization of the free layer
α_{mag}	Magnetic $1/f$ Hooge parameter

Figure 12 shows the detectivity of several commercial magnetic sensors. Also shown are our estimates of the possible performance at 0.01 Hz that may be attained using MEMS flux concentrators. The steps required are using the MEMS flux concentrator, MTJ sensors, and increasing the volume of the free layer. The most challenging step will be to increase the volume of the free layer sufficiently that the noise is not determined by the magnetic white noise. The improvements shown in Fig. 12 are based on using reasonable estimates[25] in the following equation for the noise sources:

$$S_B = \frac{4B_{\mathrm{sat}}^2}{(\Delta R/R)^2 N^2 V_J^2}\left[S_V^{\mathrm{Amp}} + N\frac{2eV_J[\mathrm{RAP}]}{A}\coth\left(\frac{eV_J[\mathrm{RAP}]}{2k_BT}\right) + N\frac{\alpha_{\mathrm{elect}}V_J^2}{Af}\right] + \frac{1}{N}\frac{4k_BT\mu_0\alpha_G}{\Omega\gamma M_s} + \frac{2B_{\mathrm{sat}}}{N}\frac{\alpha_{\mathrm{mag}}}{\Omega f}, \quad (2)$$

where the symbols are defined in Table II.

III. SUMMARY

Several approaches have been discussed for improving the performance of magnetic sensors. Although miniaturization offers potential cost savings, there are also cases where decreasing the size will also decrease the performance characteristics. For example, decreasing the volume of the cell in the chip scale magnetometers will decrease the sensitivity when collisions with the cell wall limit the spin lifetime. To take full advantage of the potential cost savings, it will be necessary to find large enough markets to justify the engineering and manufacturing cost of producing large quantities of sensors with improved performance. Trade-offs must be made. For example, it is desirable to increase the impedance of MTJ sensors to decrease the power consumption, but increasing the impedance increases the Johnson noise. Increasing the size of the MEMS flaps increases the amplitude of the field modulation in the MEMS flux concentrator and/or permits the use of larger sensors, but it also tends to decrease the resonant frequency. New total field and vector field magnetometers offer the possibility of smaller, lower cost, and/or higher sensitivity magnetic sensors. In general, these sensors will also consume less power. These positive features may give rise to new applications and create a larger market for magnetic sensors.

ACKNOWLEDGMENTS

The assistance of Kim Olver, Gail Koebke, and Manrico Mirabelli in fabricating the devices is gratefully acknowledged.

[1] J. Lenz and A. S. Edelstein, IEEE Sens. J. **6**, 631 (2006).
[2] R. C. Chavesa and P. P. Freitas, Appl. Phys. Lett. **91**, 102504 (2007).
[3] W. Happer, Rev. Mod. Phys. **44**, 169 (1972).
[4] A. W. Overhauser, Phys. Rev. **92**, 411 (1953).
[5] T. L. Francis *et al.*, New J. Phys. **6**, 185 (2004).
[6] G. Binasch *et al.*, Phys. Rev. B **39**, 4828 (1989).
[7] M. N. Baibich *et al.*, Phys. Rev. Lett. **61**, 2472 (1988).
[8] M. J. Carey *et al.*, Appl. Phys. Lett. **81**, 1044 (2002).
[9] M. Julliere, Phys. Lett. **54A**, 225 (1975).
[10] W. H. Butler *et al.*, Phys. Rev. B **63**, 054416 (2001).
[11] J. Mathon and A. Umerski, Phys. Rev. B **63**, 220403 (2001).
[12] S. S. P. Parkin *et al.*, Nat. Mater. **3**, 862 (2004).
[13] S. Yuasa, Nat. Mater. **3**, 868 (2004).
[14] C. Heiliger, P. Zahn, and I. Mertig, Mater. Today **9**, 46 (2006).
[15] D. Budker *et al.*, Rev. Mod. Phys. **74**, 1153 (2002).
[16] P. D. D. Schwindt *et al.*, Appl. Phys. Lett. **85**, 6409 (2004).
[17] S. Tumanski, *Thin Film Magnetoresistive Sensors* (IOP, Bristol, 2001), p. 125.
[18] F. C. S. d. Silva *et al.*, Appl. Phys. Lett. **85**, 6022 (2004).
[19] J. Zhai *et al.*, Appl. Phys. Lett. **89**, 083507 (2006).
[20] W. N. Podney, U.S. Patent No. 5,675,252 (Oct. 7, 1997).
[21] A. S. Edelstein *et al.*, J. Appl. Phys. **99**, 08B317 (2006).
[22] A. S. Edelstein and G. A. Fischer, J. Appl. Phys. **91**, 7795 (2002).
[23] N. Smith and P. Arnett, Appl. Phys. Lett. **78**, 1448 (2001).
[24] P. Dutta and P. M. Horn, Rev. Mod. Phys. **53**, 497 (1981).
[25] R. D. McMichael, P. Pong, J. Unguris, W. F. Egelhoff, Jr., E. R. Nowak, A. S. Edelstein, J. Burnette, and Greg Fischer (unpublished).